Title
Pair Correlation Analysis Maps the Dynamic Two-Dimensional Organization of Natural Killer Cell Receptors at the Synapse

Journal
ACS Nano, 13(12)

ISSN
1936-0851

Authors
Hedde, Per Niklas
Staaf, Elina
Singh, Sunitha Bagawath
et al.

Publication Date
2019-12-24

DOI
10.1021/acsnano.9b07486

Peer reviewed

ACS NANO

Cite This: ACS Nano 2019, 13, 14274−14282

www.acsnano.org

ARTICLE

Pair Correlation Analysis Maps the Dynamic Two-Dimensional Organization of Natural Killer Cell Receptors at the Synapse

Per Niklas Hedde,[*,†,‡] Elina Staaf,[§] Sunitha Bagawath Singh,[§] Sofia Johansson,[§] and Enrico Gratton[*,†]

[†]Laboratory for Fluorescence Dynamics, University of California Irvine, Irvine, California 92697, United States

[‡]Department of Cell and Molecular Biology, John A. Burns School of Medicine, University of Hawaii, Honolulu, Hawaii 96813, United States

[§]Department of Microbiology, Tumor and Cell Biology, Karolinska Institutet, Stockholm 17177, Sweden

Supporting Information

ABSTRACT: **In living systems, the contact between cells is the basis of recognition, differentiation, and orchestration of an immune response. Obstacles and barriers to biomolecular motion, especially for receptors at cellular synapses, critically control these functions by creating an anisotropic environment. Whereas conventional fluorescence fluctuation methods, such as fluorescence correlation spectroscopy or fluorescence recovery after photobleaching, can only measure the isotropic diffusion of molecules, the two-dimensional pair correlation function (2D-pCF) approach probes the anisotropic paths at different spatial locations within an image, allowing the creation of high-resolution maps that can visualize and quantify how molecules move in a living cell. In this work, we show how the 2D-pCF method maps the environment in cellular synapses as perceived by natural killer (NK) cell receptors. In cultured human HLA null 721.221 cells, 2D-pCF reveals the motion of inhibitory receptor HLA-Cw4-YFP coexpressed with KIR3DL1 to be highly directional around specific loci, while these restrictions were absent in the case of HLA-B51-YFP coexpressed with KIR2DL1. Further, in freshly isolated educated ($H\text{-}2D^{d}$) and uneducated ($MHC^{-/-}$) primary murine NK cells, the 2D-pCF method shows significant differences in the paths taken by activating receptor NKp46 and inhibitory receptor Ly49A in educated compared to uneducated cells. Altogether, we demonstrate that the 2D-pCF method is very powerful in informing about the spatial organization of motion in cells. Our data support the hypothesis that flexibility in the spatial arrangement of membrane receptors, that is, the absence of barriers, is crucial for NK cell function.**

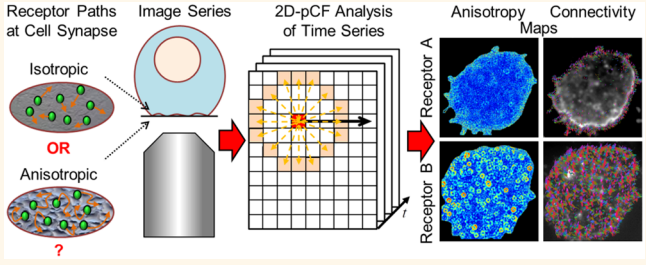

KEYWORDS: *fluorescence fluctuation spectroscopy, pair correlation analysis, natural killer cells, immune cell receptors, barrier mapping, spatiotemporal correlation*

In many natural systems, including living organisms, thermal diffusion is considered a universal isotropic transport mechanism of molecules to their target locations. Barriers to diffusion can break the symmetry and direct the flow of molecules to produce unexpected physical/biological results. In cells, such barriers to biomolecule movement can be important regulatory factors. In this work, we describe an approach to map barriers to diffusion, and we show that cellular systems, particularly at the contact between cells, are regions where these barrier structures cause symmetry breaking and anisotropic motions. The two-dimensional pair correlation function (2D-pCF) algorithm maps the paths taken by molecules within and around these structures which are key to the understanding of biological function.

Importantly, responses of immune cells are controlled by membrane receptors successfully locking to antigens presented on the surface of target cells, a process which is critically modulated by the dynamic spatial arrangement of those receptors. We and others have previously characterized the average receptor motion revealing significant differences in the isotropic movement of activating and inhibitory receptors in educated compared to uneducated NK cells.[1,2] However, the dynamic spatial organization of receptors at the immune synapse remained unclear. This is because common approaches to measure biomolecular movement either probe only a single point with limited spatial information (*e.g.*, fluorescence correlation spectroscopy (FCS) and fluorescence recovery after photobleaching (FRAP))[3,4] or measure only the

Received: September 22, 2019
Accepted: November 20, 2019
Published: November 20, 2019

DOI: 10.1021/acsnano.9b07486
ACS Nano 2019, 13, 14274−14282

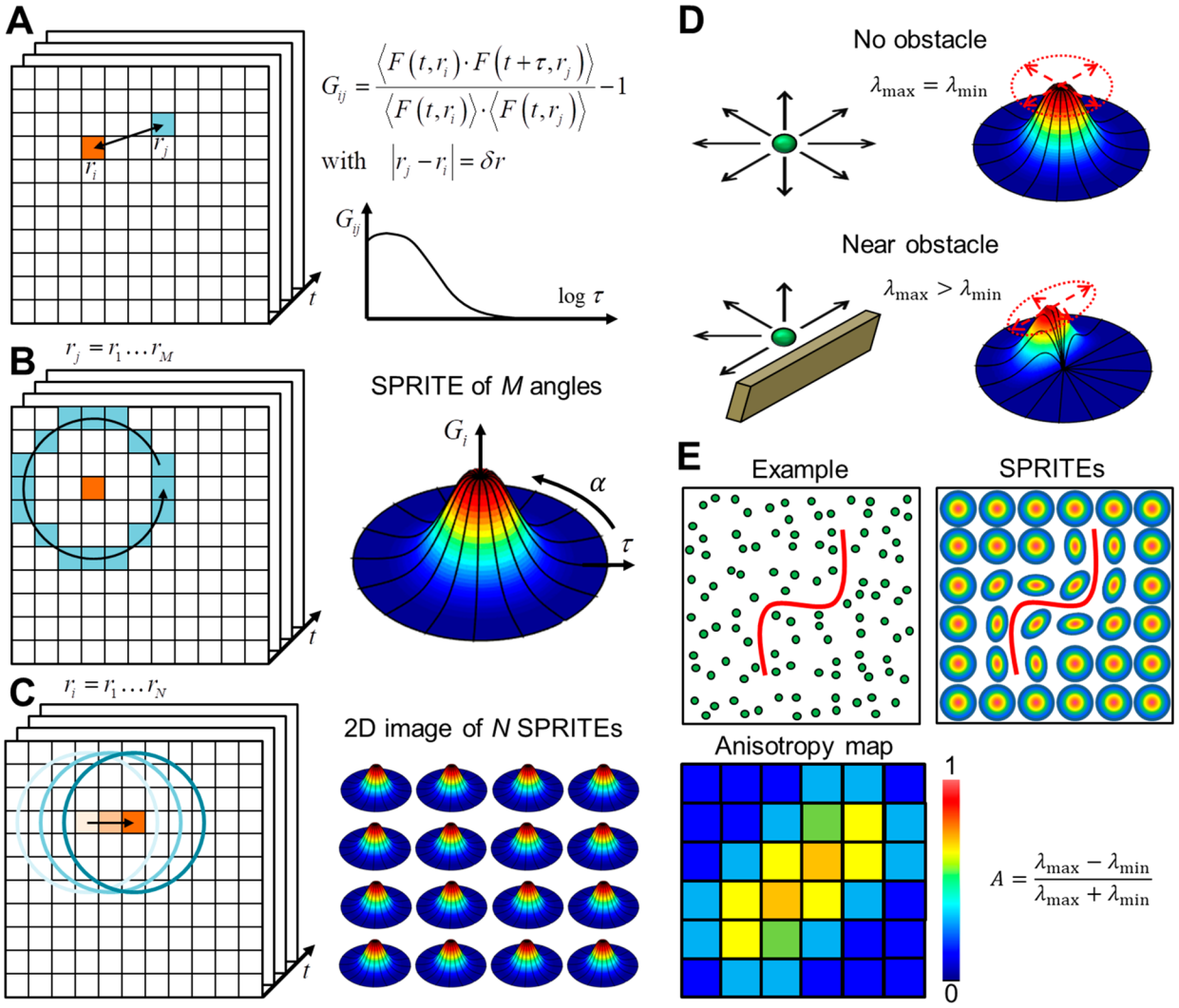

Figure 1. Principle of the 2D-pCF method. (A) Time-dependent fluorescence signal in each image pixel is correlated with the time series of the neighboring pixels at the pair correlation distance, δr. (B) For each pixel, this results in a set of correlation functions for different angles around the origin. (C) These 2D functions (SPRITEs) are calculated and stored for each image pixel. (D) If an obstacle is present within the pCF distance, the SPRITE of correlation functions is deformed, resulting in an increased anisotropy. (E) Concept of the anisotropy map. Near an obstacle, the SPRITEs get deformed, resulting in an increased anisotropy of a long (λ_{max}) and short (λ_{min}) SPRITE axis calculated by moment analysis. If the anisotropy of the SPRITE in each pixel is plotted as a heat map, underlying barriers can be visualized.

average motion over a larger region destroying information about local variations caused by an anisotropic environment (*e.g.*, RICS and image mean square displacement (iMSD)).[5,6] Consequently, local anisotropies in motion cannot be resolved by these methods, and there is no information about the shape or extension of potential barriers or channels that molecules can move in and around. Although, in principle, tracking of each molecule, or at least molecules of a given kind, could produce a map of barriers to their motion, simultaneous tracking of many molecules could be impossible given the high natural concentration in cells and the short time frame compatible with changes in motion imposed by barriers present in the membrane of live cells. Further, in addition to physical barriers, notoriously difficult to visualize thermodynamic barriers by phase separations are believed to have strong effects in cell fate and signaling.[7] To understand the spatial organization of motion, direct visualization and quantification of the paths taken by molecules in live cells is urgently needed. The 2D-pCF approach can address this need and map how molecules move in cells to study biological phenomena and to potentially accelerate drug discovery.

In the following, we demonstrate how the 2D-pCF method can visualize invisible barriers on the nanoscale and how the application of this approach can map the environment as perceived by activating and inhibitory receptors in the membrane of NK cells that play a critical role in NK cell education.

RESULTS AND DISCUSSION

2D-pCF Method Can Map the Motion of Biomolecules in Cells. In this section, we describe the physical principle and the algorithm of the 2D pair correlation function calculation. The basic idea of fluorescence fluctuation spectroscopy (FFS) methods is that fluctuations in fluorescence intensity are caused by the transit of single molecules through a small observation volume.[8] The average transit time can be quantified to measure molecule movement in a single point[3] or as an average over a larger region of interest.[5,6] Indirect

DOI: 10.1021/acsnano.9b07486
ACS Nano 2019, 13, 14274−14282

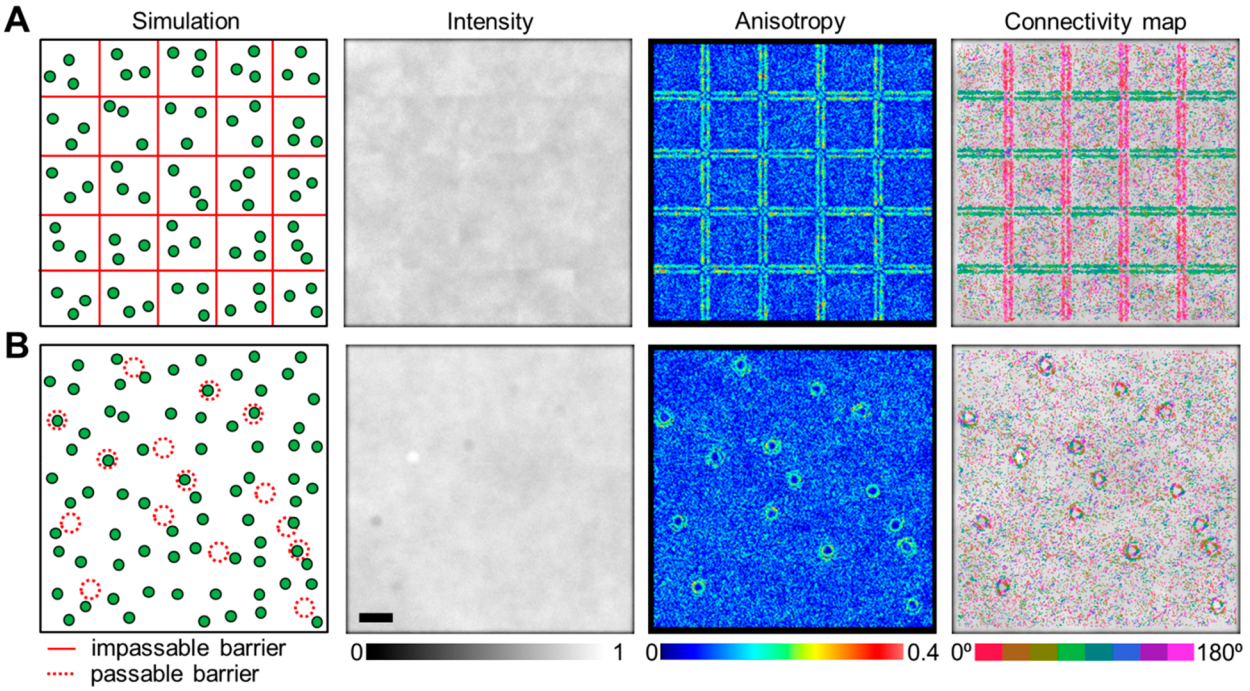

Figure 2. Simulated data. (A) Simulation of molecules diffusing at 1 μm^2 s^{-1} trapped in an invisible mesh. From the intensity image, it is not possible to make out barriers, whereas they are clearly visible in the anisotropy and connectivity maps from 2D-pCF analysis (δr = 4 pixels). (B) Simulation of molecules diffusing at 1 μm^2 s^{-1} with the possibility of becoming transiently trapped in invisible microdomains. Again, from the intensity image, it is not possible to make out the domains while they are accurately represented in the corresponding anisotropy and connectivity maps. For the connectivity maps, only pixels with anisotropies >0.1 were painted. Scale bar, 3 μm.

evidence of restricted motion or active transport can be obtained by comparing the results with the free diffusion law but lacks the ability to pinpoint their cause and spatial distribution. Instead, by (pair) correlating the fluctuations between two volumes at a given distance, we can obtain the transit probability and time between those points and any obstacle or transport channel in between will modify the time delay of this pair correlation function (pCF). As, in cells, biomolecules can translocate on the millisecond time scale, fluorescently tagged molecules must be repeatedly probed in multiple spatial locations with adequate temporal resolution to be able to apply the pCF method to the resulting data. With laser scanning microscopy, fast probing of many points can be achieved by repeatedly scanning a line across an object of interest, allowing any obstacles to molecular motion along this line to be mapped.[9] Recent advances in camera technology achieving millisecond frame readouts in combination with total internal reflection microscopy or light sheet microscopy-based optical sectioning[10,11] have made it possible to extend this principle to an entire image, as in 2D-pCF.[12] From the image time series, the time-dependent fluorescence signal in each image pixel is correlated with the time series of the neighboring pixels at the pair correlation distance, δr (Figure 1A), yielding a set of pair correlation functions for several (typically 32) equally spaced angles around the origin; if plotted as a function of time delay, τ, and angle, α, a sub image is obtained for each pixel (Figure 1B). These polar plots, in analogy to computer graphics terminology, are referred to as SPRITEs (Figure 1C). In the absence of obstacles within the pair correlation distance, the molecules can move isotropically and the correlation amplitude response, G_{ij}, will be equal in all directions, resulting in a SPRITE of round shape. Across a barrier, the communication between pixels is delayed or absent, changing the correlation functions for those angles, resulting in a deformed SPRITE (Figure 1D), which can be quantified by moment analysis in a model-free, fit-free manner. Simple metrics sensitive to both symmetric and asymmetric deformations are the anisotropy and the major axis angle of the SPRITE (Figure 1E). By color coding each pixel according to the anisotropy value and direction of the respective SPRITE, maps deciphering the labyrinth presented to the molecules of interest can be created, as simulated in Figure 2.

2D-pCF Analysis of Simulated Molecules Diffusing while Trapped in an Invisible Meshwork and in Microdomains Can Visualize the Barrier Structure. Common obstacles and barriers in cells include (transient) trapping of molecules in a meshwork and in microdomains. To investigate if the 2D-pCF approach is able to detect such barriers to moving molecules, we simulated those two scenarios. First, a plane, in which molecules can otherwise diffuse freely, was subdivided into 25 compartments by thin invisible barriers that molecules cannot cross. Molecules were seeded in those compartments at equal molecular density and free diffusion at 1 μm^2 s^{-1} was simulated; the resulting data were analyzed by the 2D-pCF method (Figure 2A). As the molecules were homogeneously distributed among compartments, the intensity projection of all frames does not show any underlying structure. Even in the presence of features with higher average intensity, it would not be clear from the image if those structures were caused by trapped but moving molecules or an unrelated static immobile fraction. To reveal barriers to moving molecules, the 2D-pCF method was applied. At a distance from any barrier larger than the pCF calculation distance, the diffusion was isotropic (round SPRITE profile, small anisotropy). Near a border at a distance smaller than the pCF calculation distance, the amplitude of the pCF decreased

DOI: 10.1021/acsnano.9b07486
ACS Nano 2019, 13, 14274−14282

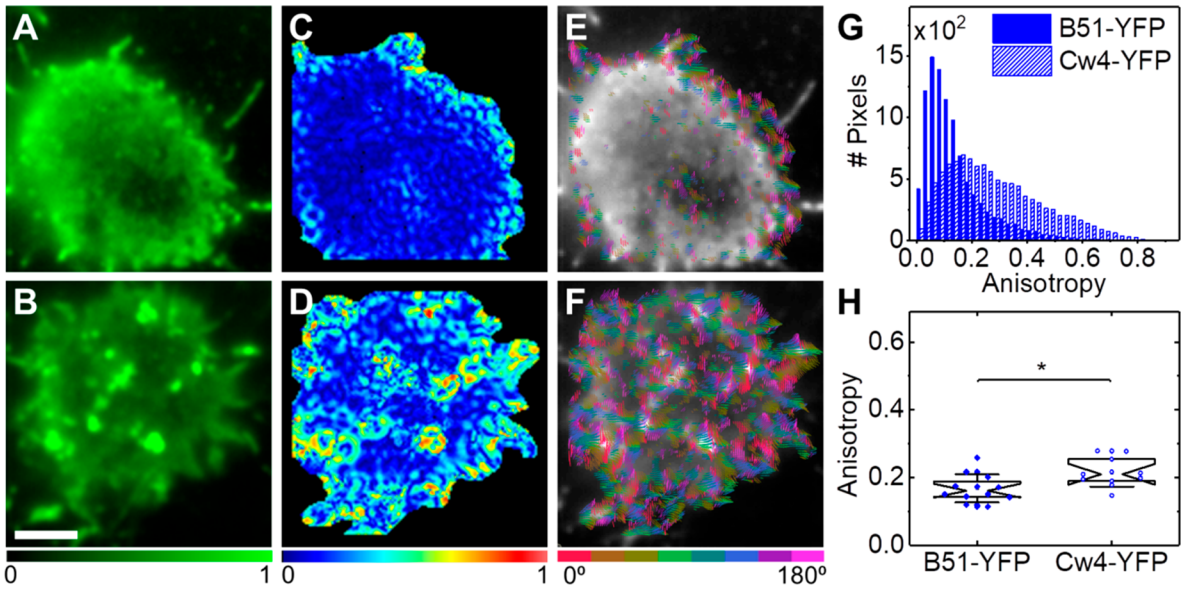

Figure 3. Cultured NK cells. (A,B) Fluorescence images of HLA-B51-YFP (A) and HLA-Cw4-YFP (B) ligands expressed together with KIR1DL2 and KIR1DL3 receptors, respectively, in cultured 721.221 cells. (C,D) Anisotropy maps of the same cells shown in (A,B) calculated for a pair correlation distance δr = 0.4 μm. (E,F) For the connectivity maps, only segments with anisotropies >0.15 were drawn on top of the grayscale fluorescence images. (G) Histograms of the anisotropy maps shown in panels (C,D). (H) Average anisotropies of 12 cells expressing HLA-B51-YFP/KIR1DL2 and 11 cells expressing HLA-Cw4-YFP/KIR1DL3. The boxes represent the median and the first and third quartiles, and the notches represent the 95% confidence intervals. The whiskers show the 95% ranges. *$P \leq 0.05$ (Mann−Whitney test). Scale bar, 3 μm.

in the direction of the barrier as the same molecule could never be observed in the other side of the barrier. The SPRITE profile was deformed in the direction of the barrier, resulting in an increased anisotropy parallel to the border of the obstacle. The same deformation occurred for molecules that arrived from the other side of the barrier. Further details of the 2D-pCF method are discussed in the Methods section and in the Supporting Information. For less restricted/directed motion, the signal-to-noise ratio of the anisotropy map generally decreases at larger pCF distances as it is less likely to find the same molecule (Figure S1). Yet, this effect is less pronounced for strongly directed motion, such as molecule movement inside a channel, where the probability for the same molecule to reappear is high even at larger pCF distances (Figure S2). In addition, as a differential measurement between pixels, the effect of fluorophore bleaching on the 2D-pCF map is minimal (Figure S3). To help visualize the effective flow of molecules near obstacles, a connectivity map is created by drawing segments of a length proportional to the pixel anisotropy on top of the intensity image (Figure S4) similarly to diffusion tensor imaging (DTI) in magnetic resonance imaging (MRI).[13] The connectivity map is a convenient way to convey the information on the anisotropy amplitude and direction in a single map that highlights areas of strongly directional/confined molecule movement. We note that the connectivity map is used for visualization only and not for statistical data analysis. For the second scenario of molecules transiently trapped in microdomains, we created 1 μm diameter domains that nearby molecules can enter and, once trapped, leave with 1% probability per simulated frame (Figure 2B). Again, the intensity projection could not be used to reliably identify the domains as the molecules were homogeneously distributed, but the domain outlines are clearly visible in the anisotropy image and the flow of molecules around the domains is accurately represented in the connectivity map. In Figure S5, we added regions of higher intensity representing immobile fractions to the simulation to demonstrate that those do not interfere with 2D-pCF analysis. The molecule concentration suitable for 2D-pCF analysis is in alignment with the range of other FFS methods (~0.1−200 nM) and strongly depends on the fluorophore brightness as well as the amplitude of other signal fluctuations such as detector/amplifier noise and laser fluctuations.[14−16] From simulations, where only shot noise was added, which does not correlate, it can be seen that the number of molecules does not affect the signal-to-noise ratio of the anisotropy maps at all. The number of frames analyzed, however, has a profound effect on the signal-to-noise (Figure S6). Hence, for weakly fluorescent molecules, the number of frames collected must be increased to yield high contrast anisotropy maps. Collecting a large number of frames can also allow for the observation of changes in obstacles/barriers such as induced in cells by a drug. To analyze, the large time series can be subdivided into smaller parts using a sliding window. As an example, the appearance of barriers was simulated in Figure S7.

Barriers to NK Cell Receptor Motion in Cell Lines Revealed by the 2D-pCF Method. A rapidly growing research focus area is the distribution of receptors in immune cells as they have shown great potential to be exploited for cancer immunotherapy,[17] and their distribution and dynamics remain a major unsolved problem. For example, antibodies administered to patients blocking inhibitory T-cell receptors were able to unleash the immune system toward tumor regression.[18,19] Natural killer cells are an important class of cytotoxic lymphocytes that can provide an innate immune response to control infections and to provide tumor immunosurveillance.[20,21] NK cells have been increasingly utilized in cancer therapy, as well, especially for the treatment of blood cancers, however, with mixed results.[22−24] A major determinant of NK cell responsiveness toward target cells is

DOI: 10.1021/acsnano.9b07486
ACS Nano 2019, 13, 14274−14282

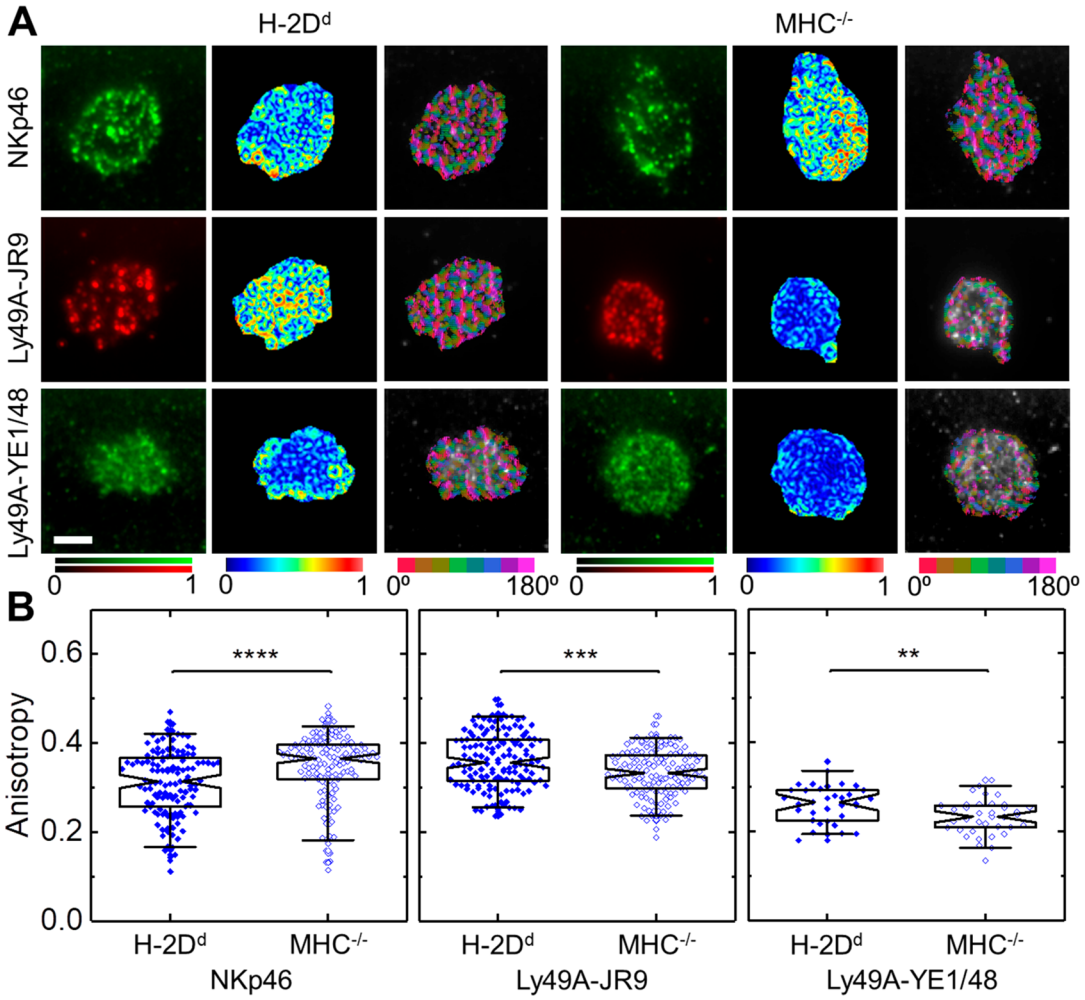

Figure 4. Primary murine NK cells. (A) Fluorescence images and corresponding anisotropy and connectivity maps of activating NKp46 and inhibitory Ly49A receptors labeled with dye-conjugated antibodies in educated ($H\text{-}2D^d$) and uneducated ($MHC^{-/-}$) primary murine NK cells ($\delta r = 0.4\ \mu m$). For the connectivity map, only segments with anisotropies >0.2 were drawn on top of the grayscale fluorescence images. (B) Statistical analysis of the anisotropy of 129/138 (NKp46), 145/137 (Ly49A-JR9), and 35/37 (Ly49A-YE1/48) $H\text{-}2D^d/MHC^{-/-}$ cells from 12 (NKp46), 11 (Ly49A-JR9), and 3 (Ly49A-YE1/48) independent experiments. Each point represents the average anisotropy of a single cell. The boxes represent the median and the first and third quartiles, and the notches represent the 95% confidence intervals. The whiskers show the 95% ranges. $^{**}P \leq 0.01$, $^{***}P \leq 0.001$, $^{****}P \leq 0.0001$ (Mann−Whitney test). Scale bar, 3 μm.

NK cell education,[25] a process poorly understood today. The key to unraveling many of the underlying mechanisms is to get a better grasp of dynamic receptor organization including symmetry breaks in their motion. Therefore, we applied the 2D-pCF method to study the environment as perceived by membrane receptors at the synapse of NK cells. NK cells have different MHC class I allelic specificity for missing-self-killing and education ensures that only NK cells with self-specific inhibitory receptors can respond.[26−28] Stronger responses are kept in check by inhibitory receptors that recognize MHC-I ligands on most somatic cells including the killer cell Ig-like receptor (KIR) family on human NK cells.[29] Nomenclature is based on KIRs having either two extracellular Ig-like domains (2D) or three extracellular Ig-like domains (3D) and long (L) or short cytoplasmic tails (S). In general, the KIR-L types are inhibitory, whereas the KIR-S types are activating receptors.[30] The ratio of activating to inhibitory signals received from cell surface receptors that bind to ligands on neighboring cells determines NK cell activation status.[31] We investigated inhibitory receptors KIR2DL1 and KIR3DL1 in HLA null 721.221 cells from lymphoma background. These cells lack surface expression of any surface HLA or inhibitory/activating receptors and, for the study, have been retransfected with combinations of KIR2DL1 together with HLA-B51-YFP as well as KIR3DL1 together with HLA-Cw4-YFP. The cell membrane at the immune synapse was imaged repeatedly by total internal reflection (TIRF) microscopy[10] to acquire data suitable for 2D-pCF analysis. The normalized sums of exemplary image sequences are shown in Figure 3A for HLA-B51-YFP and in Figure 3B for HLA-Cw4-YFP. Whereas B51-YFP seemed to be more evenly distributed throughout the membrane than Cw4-YFP, it is not possible to draw any conclusions about barriers, dynamic binding, and/or confinement from the fluorescence images. Application of 2D-pCF analysis to the data, on the other hand, produced anisotropy maps (Figure 3C,D) and connectivity maps (Figure 3E,F) that clearly revealed a much higher level of anisotropic motion for HLA-Cw4-YFP compared to HLA-B51-YFP with a highly directional flow around certain loci. Masking was applied to specifically select the portion of the images that show NK cells.[32,33] The anisotropy distributions of the maps are plotted in Figure 3G, and statistical analysis of the average anisotropies

DOI: 10.1021/acsnano.9b07486
ACS Nano 2019, 13, 14274−14282

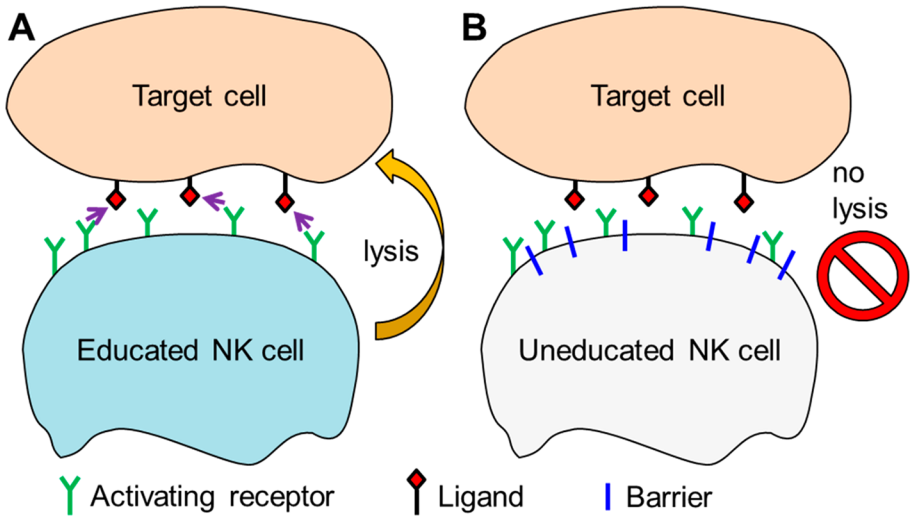

Figure 5. Model of activating receptor spatial dynamics in educated *vs* uneducated NK cells.

of 11/12 cells per receptor/ligand combination proved to be significantly different (Figure 3H). A more isotropic motion of HLA-B51-YFP expressed in cells co-transfected with KIR2DL1 was expected as KIR2DL1 is known to bind HLA-C allotypes but not HLA-B molecules.[34,35] On the contrary, the highly directional flow around certain loci of HLA-Cw4-YFP expressed in cells co-transfected with KIR3DL1 indicative of tethering points is more surprising, as KIR3DL1 is known to bind HLA-B allotypes such as Bw4 but not HLA-C allotypes including Cw4.[34] A similar trend in anisotropy maps was observed for antibody-labeled KIRs in HLA-B51-YFP compared to HLA-Cw4-YFP expressing cells (Figure S8). Recent literature shows that KIR3DL1 exhibits weak but significant binding to a wider range of class I HLA molecules.[36] This effect is possibly attributed to D0, the first of the three Ig domains of KIR3DL1, which has been found to recognize even nonclassical MHC-I molecules such as HLA-G, suggesting that MHC-I could bridge several KIR3DL1 molecules together in a way to facilitate signaling.[37]

In Primary Murine NK Cells, Barriers to Diffusion Inhibit Activating Receptor Motion in Uneducated Cells and Inhibitory Receptor Motion in Educated Cells. The murine equivalents of human KIRs are the Ly49 family of receptors which represents the most thoroughly studied inhibitory receptor family in mice. Subsets of NK cells displaying different combinations of Ly49 family members are produced by stochastic expression of the genes encoding these receptors leading to individual NK cells having different MHC class I allelic specificity for which they perform missing-self-killing. Not all NK cells have an inhibitory receptor that recognizes a self MHC class I allele, and NK cells undergo an educational process to ensure that only NK cells with self-specific inhibitory receptors are able to perform missing-self-killing. NK cells without self-specific inhibitory receptors are hyporesponsive in the resting state.[28] We and others previously quantified inhibitory and activating receptor dynamics in educated compared to uneducated primary murine NK cells using conventional FFS-based techniques as well as single-particle tracking;[1,2] educated NK cells showed faster movement of the activating receptor NKp46 and confinement of the inhibitory receptor Ly49A.[2] However, the mechanism behind these differences in terms of molecule dynamics remains elusive as common FFS methods lack spatial information and struggle to provide detailed insight into what is causing the observed differences in dynamics. Here, we analyzed the same data acquired by means of TIRF microscopy with the 2D-pCF method; exemplary fluorescence images and corresponding maps of anisotropy and connectivity are shown in Figure 4A, and all data are quantified in Figure 4B; the effect of the pair correlation distance is discussed in Figure S9. Again, masking was applied to specifically select the portion of the images that show NK cells. The differences in anisotropy maps between freshly isolated educated ($H\text{-}2D^d$) and uneducated ($MHC^{-/-}$) cells are striking. For the activating receptor, NKp46, the presence of very dense networks of obstacles are indicated in uneducated cells while mostly absent in educated cells. For the inhibitory receptor, Ly49A, the situation is reversed with more obstacles in educated cells. These findings strongly support our hypothesis that flexibility in spatial arrangement of membrane receptors, that is, the absence of barriers, is crucial for NK cell responsiveness. Activating receptors can be spatially rearranged quicker in educated NK cells as binding to the antigens presented on the membrane surface of target cells should occur in a rapid fashion (Figure 5), whereas inhibitory receptor arrangement is more rigid. We speculate that higher flexibility in activating receptor rearrangement facilitates binding to target cell antigens such that educated NK cells can initiate target cell lysis more efficiently (Figure 5). As uneducated NK cells should remain hyporesponsive, antigen binding is less efficient with barriers preventing quick spatial rearrangement of activating receptors. A more restricted movement of Ly49A was anticipated given that it binds to $H\text{-}2D^d$ on educated cells. Uneducated NK cells exhibit an inverted behavior as they should remain hyporesponsive.

CONCLUSIONS

Overall, we showed that the 2D-pCF method is a very powerful approach to inform about biomolecular dynamics from a different angle; by leveraging signal fluctuations caused by molecule movement from one spatial location to another, it is possible to paint a picture of their surroundings rather than, or, in addition to, focusing on the average movement. As demonstrated for NK cell receptors, barriers and obstacles causing anisotropic motion can be directly visualized and quantified by the 2D-pCF approach. We found that, in 721.221

DOI: 10.1021/acsnano.9b07486
ACS Nano 2019, 13, 14274−14282

cells, the motion of HLA-Cw4-YFP coexpressed with KIR3DL1 was highly directed around specific loci compared to HLA-B51-YFP coexpressed with KIR2DL1, possibly due to HLA-Cw4-YFP binding to KIR3DL1. Further, in primary murine NK cells, the dynamics of activating receptor NKp46 and inhibitory receptor Ly49A were found to strongly depend on NK cell education status. A more isotropic motion of the activating receptor NKp46 was observed in educated cells, whereas, for the inhibitory receptor Ly49A, the motion in educated cells was more anisotropic compared to that in uneducated cells. Importantly, the application of the 2D-pCF method is not limited to membrane receptors but can be applied to many other areas including the cell cytoplasm, the nucleus, and cell−cell contacts. Finally, we want to emphasize that data acquired for analysis with conventional FFS methods such as iMSD[6,38] analysis is usually compatible with 2D-pCF analysis and *vice versa*. As such, we believe that the 2D-pCF method will greatly enrich the toolbox to visualize, quantify, and understand biomolecular dynamics in living cells on the nanoscale.

METHODS

Simulated Data. We simulated molecules moving in a plane with molecule movement restricted by invisible barriers to illustrate the concept of 2D-pCF analysis. Data were simulated with a Matlab script. A total of 5000−10000 molecules were seeded in a plane of 256 × 256 pixels by plotting a Gaussian intensity distribution of 2.5 pixels width for each molecule. Pixel size was set to 100 nm. Each molecule was randomly displaced by application of the diffusion law in two dimensions at 1 $\mu m^2\ s^{-1}$ at 10 ms intervals, simulating a camera frame rate of 100 frames per second. Each image frame was normalized to one and Gaussian noise (Matlab function imnoise-(I,'Gaussian')) with a variance of 0.1 was added followed by rescaling to the 16 bit range of the TIFF image format. To simulated trapping in a meshwork, the plane was subdivided into 5 by 5 compartments that molecules cannot cross. For Figure 2A, 200 molecules were seeded in each compartment to yield a homogeneous intensity distribution. For Figure S1, the simulation was repeated with randomly seeded molecules and with the addition of a molecule off rate that permanently removes molecules with 0.0001 probability for each simulated frame. To simulate transient trapping in microdomains (Figure 2B), 15 domains of 10 pixel diameter were added to the simulated plane, and molecules at those domains were assigned a 1% probability to enter and 1% probability to leave, once entered, per frame. For Figure S5, the microdomain simulation was repeated adding 10 randomly placed 20 pixel diameter regions of constant amplitude to represent immobile fractions, for example, caused by autofluorescence in cells. A total of 10000 frames were simulated for each image data set. Each simulation was equilibrated for 1000 frames before recording data.

2D-pCF Analysis. A detailed description of the 2D-pCF method can be found in Malacrida *et al.*[12] Briefly, the 2D-pCF function defined as

$$G_{ij} = \frac{\langle F(t, r_i)\cdot F(t+\tau, r_j)\rangle}{\langle F(t, r_i)F(t, r_j)\rangle} - 1 \tag{1}$$

was calculated for each pixel where τ is the time delay between acquisition of the fluorescence intensity, F, at two points, r_i and r_j, with distance, $\delta r = |r_j - r_i|$, in the image; the temporal average is indicated by brackets. The pCFs were logarithmically averaged using 32 equally logarithmic spaced time intervals. A maximum of the correlation function will appear at a time delay proportional to the average time it takes a molecule to move between the two points. In the presence of an obstacle between the two points, molecules will need to go around and it will take them longer to appear at the other location, if it can be reached at all. This way, 2D-pCF detects barriers to molecular motion and heterogeneity as the time of the correlation maximum is delayed in the presence of barriers. By following the same molecule over a large area a map of molecular diffusion can be produced. As all fluctuation spectroscopy methods, 2D-pCF does not require isolated molecules, which is an inherent advantage over single-particle tracking methods. Many molecules can be labeled with the same fluorophore and be located within the same volume of observation. For the analysis, a set of correlation functions (SPRITE, 32 × 32 pixels) for different equally spaced angles (we generally use 32 angles, but the number is adjustable) around the origin was calculated. If the molecules move isotropically, the correlation amplitude response caused by molecule movement between pixels separated by δr is equal in all directions, whereas the SPRITE is deformed when there is an obstacle to diffusion within the distance analyzed. To quantify this deformation, we calculated the zero-, first-, and second-order moments in x and y direction (indexed p,q) for each SPRITE using

$$\mu_{pq} = \sum_x \sum_y (x-\bar{x})^p (y-\bar{y})^q G(x, y) \tag{2}$$

Bars denote spatial averages. From those moments, the minor and major axes, λ_{min} and λ_{max}, were obtained with

$$\lambda_{max,min} = \frac{\mu_{20}+\mu_{02}}{2} \pm \frac{\sqrt{4\mu_{11}^2 + (\mu_{20}-\mu_{02})^2}}{2} \tag{3}$$

We defined the anisotropy indicating the degree of SPRITE deformation as

$$A = \frac{\lambda_{max} - \lambda_{min}}{\lambda_{max} + \lambda_{min}} \tag{4}$$

The angle of the major axis was obtained from the moments with

$$\varphi = \frac{1}{2}\tan^{-1}\left(\frac{2\mu_{11}}{\mu_{20}-\mu_{02}}\right) \tag{5}$$

We note that neither of the above parameters require any prior information nor do they assume any model as their calculation is fit-free.

Masking. In the absence of signal, the correlation function (eq 1) will produce near-zero values as noise does not correlate. However, those small random values will give rise to large anisotropy values and random angles. Therefore, image regions not containing a cell were excluded from 2D-pCF analysis by drawing a mask along the border of each cell. The cell outline was determined from the intensity average by the user of the software. This feature is part of the SimFCS software and is used for many other types of analyses including fluorescence lifetime imaging, for example, see Lou *et al.*[32] and Cinco *et al.*[33]

Cell Lines. The 721.221 cell line (of human origin) was cultured at 37 °C in 7.5% CO_2 in Iscove's modified Dulbecco's medium (HyClone) supplemented with 10% fetal bovine serum (FBS), 100 mg/mL penicillin−streptomycin, 5% nonessential amino acids, 0.25 mM sodium pyruvate, and 2 mM β-mercaptoethanol.

Transgene Construction. The HLA-B*5101 (referred to as B51) open reading frame was amplified by polymerase chain reaction (PCR) from plasmid IHW10033 (International Histocompatibility Working Group Genebank). The PCR product was cloned into a pCR3 vector and sequenced to ensure identity with the published sequence. The YFP open reading frame was inserted in frame at the C terminus of HLA-B51, and the HLA-B51-YFP fusion gene was subcloned into a pRRLsin.PPTshCMV.pre (Lenti) vector. Lentiviruses were produced using standard techniques and used to infect the 721.221 human cell line that does not have HLA on their surface.[39] Transduced cells were purified using flow sorting based on enhanced YFP fluorescence. The 721.221 HLA-B51-YFP cells had also been transduced with KIR2DL1. KIR2DL1 was amplified by PCR from complementary DNA prepared from YTS 2DL1 cells (provided by D. Burshtyn) and cloned into a pRRLsin.PPT.pgk.pre vector. Lentivi-

DOI: 10.1021/acsnano.9b07486
ACS Nano 2019, 13, 14274−14282

ruses were used to infect 721.221 HLA-B51-YFP cells, and transduced cells were purified using a KIR2DL1 monoclonal antibody (HP 3E4) and flow sorting. The procedure was repeated accordingly for HLA-Cw4-YFP and KIR3DL1.

Primary NK Cells. A detailed description of mice, NK cell isolation from splenocytes, antibodies and preparation of cells for imaging and spectroscopy, and TIRF microscopy can be found in Staaf *et al.*[2] Briefly, hyporesponsive NK cells were obtained from *B6.K*$^{b-/-}$*D*$^{b-/-}$ mice (here called *MHC*$^{-/-}$ mice). Educated NK cells were from *B6.K*$^{b-/-}$*D*$^{b-/-}$*D*$^{d+/+}$ mice (here called *H-2D*^{d} mice). Mouse spleens were mechanically homogenized for single-cell suspension. Erythrocytes were lysed, and splenocyte single-cell suspensions were obtained by filtration. NK cells were subsequently enriched by MACS NK cell isolation. Clone JR9.318, an antibody that recognizes Ly49A, was purified from hybridoma supernatants and conjugated to Abberior STAR 635 NHS dye (Abberior GmbH). The antibody recognizing NKp46 (clone 29A1.4, BioLegend) was conjugated to MFP488-NHS (MoBiTec GmbH). The antibody recognizing Ly49A clone YE1/48.10.6-FITC was purchased from BioLegend. Fc receptors were blocked in 16% mouse serum in phosphate buffered saline (PBS) before antibody labeling. NK cells were stained in solution, centrifuged (450g for 3 min), and resuspended in a 1:1 mixture of transparent RPMI 1640 (PAA The Cell Culture Company) and PBS with 0.5% FBS before transfer to poly-L-lysine-coated dishes with glass bottoms (MatTek Corporation, P35G-1.5-14.C; Greiner Bio-One, 627861).

Fluorescence Microscopy. For imaging of NK cell receptors at the membrane, we used total internal reflection microscopy setup on a Zeiss Elyra PS1 microscope with ZEN 2012 Black software. An alpha Plan-Apochromat 100× oil immersion objective of numerical aperture 1.46 was used for imaging, and fluorescence was excited with 488 and 633 nm laser light and detected in two channels (band-pass filter, 495 to 575 nm; long-pass filter, 655 nm) with an electron-multiplying charge-coupled device camera (Andor iXon 897) at 36 ms frame-to-frame intervals; sequences of 6000 frames were acquired per cell. Image size was 12.8 μm with 128 × 128 pixels recorded at 100 nm pixel size.

ASSOCIATED CONTENT

Supporting Information

The Supporting Information is available free of charge at https://pubs.acs.org/doi/10.1021/acsnano.9b07486.

Supplementary Figures S1−S9 (PDF)

AUTHOR INFORMATION

Corresponding Authors

*E-mail: phedde@uci.edu.

*E-mail: egratton@uci.edu (lead contact).

ORCID

Enrico Gratton: 0000-0002-6450-7391

Author Contributions

P.N.H., E.G., S.J., and E.S. conceived the project. E.S., S.B.S., and P.N.H. prepared samples and acquired imaging data. P.N.H. analyzed the data. E.G. implemented the software. P.N.H. wrote the manuscript. E.G. and S.J. supervised the project.

Notes

The authors declare no competing financial interest.

ACKNOWLEDGMENTS

We thank C. Gohlke (LFD, UCI, USA) for optimizing the 2D-pCF routine. We also want to express our gratitude to H. Blom (SciLifeLab, KI, Sweden) for helping to setup the TIRF microscope. This work was supported by NIH grants P50 GM076516 and P41 GM103540, Vetenskapsrådet, Vinnova the Swedish agency for innovation systems, Selma Andersons stipend fund, Hierta-Reitzius stipend fund, The Swedish Foundation for International Cooperation in Research and Higher Education.

REFERENCES

(1) Guia, S.; Jaeger, B. N.; Piatek, S.; Mailfert, S.; Trombik, T.; Fenis, A.; Chevrier, N.; Walzer, T.; Kerdiles, Y. M.; Marguet, D.; Vivier, E.; Ugolini, S. Confinement of Activating Receptors at the Plasma Membrane Controls Natural Killer Cell Tolerance. *Sci. Signaling* **2011**, *4*, ra21.

(2) Staaf, E.; Hedde, P. N.; Bagawath Singh, S.; Piguet, J.; Gratton, E.; Johansson, S. Educated Natural Killer Cells Show Dynamic Movement of the Activating Receptor NKp46 and Confinement of the Inhibitory Receptor Ly49A. *Sci. Signaling* **2018**, *11*, No. eaai9200.

(3) Magde, D.; Elson, E.; Webb, W. W. Thermodynamic Fluctuations in a Reacting System Measurement by Fluorescence Correlation Spectroscopy. *Phys. Rev. Lett.* **1972**, *29*, 705−708.

(4) Axelrod, D.; Koppel, D. E.; Schlessinger, J.; Elson, E.; Webb, W. W. Mobility Measurement by Analysis of Fluorescence Photobleaching Recovery Kinetics. *Biophys. J.* **1976**, *16*, 1055−1069.

(5) Digman, M. A.; Brown, C. M.; Sengupta, P.; Wiseman, P. W.; Horwitz, A. R.; Gratton, E. Measuring Fast Dynamics in Solutions and Cells with a Laser Scanning Microscope. *Biophys. J.* **2005**, *89*, 1317−1327.

(6) Di Rienzo, C.; Gratton, E.; Beltram, F.; Cardarelli, F. Fast Spatiotemporal Correlation Spectroscopy to Determine Protein Lateral Diffusion Laws in Live Cell Membranes. *Proc. Natl. Acad. Sci. U. S. A.* **2013**, *110*, 12307−12312.

(7) Alberti, S.; Gladfelter, A.; Mittag, T. Considerations and Challenges in Studying Liquid-Liquid Phase Separation and Biomolecular Condensates. *Cell* **2019**, *176*, 419−434.

(8) Tetin, S. Y. *Methods in Enzymology. Fluorescence Fluctuation Spectroscopy (FFS), Part A*; Academic Press: Oxford, 2013.

(9) Hinde, E.; Cardarelli, F.; Digman, M. A.; Gratton, E. *In Vivo* Pair Correlation Analysis of EGFP Intranuclear Diffusion Reveals DNA-Dependent Molecular Flow. *Proc. Natl. Acad. Sci. U. S. A.* **2010**, *107*, 16560−16565.

(10) Axelrod, D. Cell-Substrate Contacts Illuminated by Total Internal Reflection Fluorescence. *J. Cell Biol.* **1981**, *89*, 141−145.

(11) Huisken, J.; Swoger, J.; Del Bene, F.; Wittbrodt, J.; Stelzer, E. H. K. Optical Sectioning Deep inside Live Embryos by Selective Plane Illumination Microscopy. *Science* **2004**, *305*, 1007−1009.

(12) Malacrida, L.; Hedde, P. N.; Ranjit, S.; Cardarelli, F.; Gratton, E. Visualization of Barriers and Obstacles to Molecular Diffusion in Live Cells by Spatial Pair-Cross-Correlation in Two Dimensions. *Biomed. Opt. Express* **2018**, *9*, 303−321.

(13) O'Donnell, L. J.; Westin, C. F. An Introduction to Diffusion Tensor Image Analysis. *Neurosurg. Clin. N. Am.* **2011**, *22*, 185−196.

(14) Laurence, T. A.; Ly, S.; Bourguet, F.; Fischer, N. O.; Coleman, M. A. Fluorescence Correlation Spectroscopy at Micromolar Concentrations without Optical Nanoconfinement. *J. Phys. Chem. B* **2014**, *118*, 9662−9667.

(15) Koppel, D. E. Statistical Accuracy in Fluorescence Correlation Spectroscopy. *Phys. Rev. A: At., Mol., Opt. Phys.* **1974**, *10*, 1938−1945.

(16) Kask, P.; Günther, R.; Axhausen, P. Statistical Accuracy in Fluorescence Fluctuation Experiments. *Eur. Biophys. J.* **1997**, *25*, 163−169.

(17) Sanmamed, M. F.; Chen, L. A Paradigm Shift in Cancer Immunotherapy: From Enhancement to Normalization. *Cell* **2018**, *175*, 313−326.

(18) Phan, G. Q.; Yang, J. C.; Sherry, R. M.; Hwu, P.; Topalian, S. L.; Schwartzentruber, D. J.; Restifo, N. P.; Haworth, L. R.; Seipp, C. A.; Freezer, L. J.; Morton, K. E.; Mavroukakis, S. A.; Duray, P. H.; Steinberg, S. M.; Allison, J. P.; Davis, T. A.; Rosenberg, S. A. Cancer Regression and Autoimmunity Induced by Cytotoxic T Lymphocyte-Associated Antigen 4 Blockade in Patients with Metastatic Melanoma. *Proc. Natl. Acad. Sci. U. S. A.* **2003**, *100*, 8372−8377.

DOI: 10.1021/acsnano.9b07486
ACS Nano 2019, 13, 14274−14282

(19) Seidel, J. A.; Otsuka, A.; Kabashima, K. Anti-PD-1 and Anti-CTLA-4 Therapies in Cancer: Mechanisms of Action, Efficacy, and Limitations. *Front. Oncol.* **2018**, *8*, 86.
(20) Tu, M. M.; Mahmoud, A. B.; Wight, A.; Mottashed, A.; Bélanger, S.; Rahim, M. M. A.; Abou-Samra, E.; Makrigiannis, A. P. Ly49 Family Receptors Are Required for Cancer Immunosurveillance Mediated by Natural Killer Cells. *Cancer Res.* **2014**, *74*, 3684−3694.
(21) Jost, S.; Altfeld, M. Control of Human Viral Infections by Natural Killer Cells. *Annu. Rev. Immunol.* **2013**, *31*, 163−194.
(22) Koh, C. Y.; Ortaldo, J. R.; Blazar, B. R.; Bennett, M.; Murphy, W. J. NK-Cell Purging of Leukemia: Superior Antitumor Effects of NK Cells H2 Allogeneic to the Tumor and Augmentation with Inhibitory Receptor Blockade. *Blood* **2003**, *102*, 4067−4075.
(23) Ruggeri, L.; Capanni, M.; Urbani, E.; Perruccio, K.; Shlomchik, W. D.; Tosti, A.; Posati, S.; Rogaia, D.; Frassoni, F.; Aversa, F.; Martelli, M. F.; Velardi, A. Effectiveness of Donor Natural Killer Cell Aloreactivity in Mismatched Hematopoietic Transplants. *Science* **2002**, *295*, 2097−2100.
(24) Handgretinger, R.; Lang, P.; André, M. C. Exploitation of Natural Killer Cells for the Treatment of Acute Leukemia. *Blood* **2016**, *127*, 3341−3349.
(25) He, Y.; Tian, Z. NK Cell Education *via* Nonclassical MHC and Non-MHC Ligands. *Cell. Mol. Immunol.* **2017**, *14*, 321−330.
(26) Kärre, K.; Ljunggren, H. G.; Piontek, G.; Kiessling, R. Selective Rejection of H-2-Deficient Lymphoma Variants Suggests Alternative Immune Defence Strategy. *Nature* **1986**, *319*, 675−678.
(27) Fernandez, N. C.; Treiner, E.; Vance, R. E.; Jamieson, A. M.; Lemieux, S.; Raulet, D. H. A Subset of Natural Killer Cells Achieves Self-Tolerance without Expressing Inhibitory Receptors Specific for Self-MHC Molecules. *Blood* **2005**, *105*, 4416−4423.
(28) Kim, S.; Poursine-Laurent, J.; Truscott, S. M.; Lybarger, L.; Song, Y.-J.; Yang, L.; French, A. R.; Sunwoo, J. B.; Lemieux, S.; Hansen, T. H.; Yokoyama, W. M. Licensing of Natural Killer Cells by Host Major Histocompatibility Complex Class I Molecules. *Nature* **2005**, *436*, 709−713.
(29) Parham, P. MHC Class I Molecules and KIRS in Human History, Health and Survival. *Nat. Rev. Immunol.* **2005**, *5*, 201−214.
(30) Bashirova, A. A.; Martin, M. P.; McVicar, D. W.; Carrington, M. The Killer Immunoglobulin-Like Receptor Gene Cluster: Tuning the Genome for Defense. *Annu. Rev. Genomics Hum. Genet.* **2006**, *7*, 277−300.
(31) Lanier, L. L. NK Cell Recognition. *Annu. Rev. Immunol.* **2005**, *23*, 225−274.
(32) Lou, J.; Scipioni, L.; Wright, B. K.; Bartolec, T. K.; Zhang, J.; Masamsetti, V. P.; Gaus, K.; Gratton, E.; Cesare, A. J.; Hinde, E. Phasor Histone FLIM-FRET Microscopy Quantifies Spatiotemporal Rearrangement of Chromatin Architecture during the DNA Damage Response. *Proc. Natl. Acad. Sci. U. S. A.* **2019**, *116*, 7323−7332.
(33) Cinco, R.; Digman, M. A.; Gratton, E.; Luderer, U. Spatial Characterization of Bioenergetics and Metabolism of Primordial to Preovulatory Follicles in Whole *Ex Vivo* Murine Ovary. *Biol. Reprod.* **2016**, *95*, 129.
(34) Manser, A. R.; Weinhold, S.; Uhrberg, M. Human KIR Repertoires: Shaped by Genetic Diversity and Evolution. *Immunol. Rev.* **2015**, *267*, 178−196.
(35) Fan, Q. R.; Long, E. O.; Wiley, D. C. Crystal Structure of the Human Natural Killer Cell Inhibitory Receptor KIR2DL1-HLA-Cw4 Complex. *Nat. Immunol.* **2001**, *2*, 452−460.
(36) Saunders, P. M.; Pymm, P.; Pietra, G.; Hughes, V. A.; Hitchen, C.; O'Connor, G. M.; Loiacono, F.; Widjaja, J.; Price, D. A.; Falco, M.; Mingari, M. C.; Moretta, L.; McVicar, D. W.; Rossjohn, J.; Brooks, A. G.; Vivian, J. P. Killer Cell Immunoglobulin-Like Receptor 3DL1 Polymorphism Defines Distinct Hierarchies of HLA Class I Recognition. *J. Exp. Med.* **2016**, *213*, 791−807.
(37) Fu, L.; Hazes, B.; Burshtyn, D. N. The First Ig Domain of KIR3DL1 Contacts MHC Class I at a Secondary Site. *J. Immunol.* **2011**, *187*, 1816−1825.
(38) Hedde, P. N.; Stakic, M.; Gratton, E. Rapid Measurement of Molecular Transport and Interaction inside Living Cells Using Single Plane Illumination. *Sci. Rep.* **2015**, *4*, 7048.
(39) Shimizu, Y.; DeMars, R. Production of Human Cells Expressing Individual Transferred HLA-A,-B,-C Genes Using an HLA-A,-B,-C Null Human Cell Line. *J. Immunol.* **1989**, *142*, 3320−3328.

DOI: 10.1021/acsnano.9b07486
ACS Nano 2019, 13, 14274−14282